

Modeling of Measurement-based Quantum Network Coding on IBMQ Devices

Poramet Pathumsoot,^{*} Takaaki Matsuo,[†] Takahiko Satoh,[‡]
 Michal Hajdušek,[†] Sujin Suwanna,^{*} and Rodney Van Meter[‡]
 (Dated: December 21, 2024)

Quantum network coding has been proposed to improve resource utilization to support distributed computation but has not yet been put in to practice. We implement quantum network coding on an IBMQ processor, building two crossing Bell pairs from a single 6-qubit cluster state. We compare quantum network coding to entanglement swapping and a simple linear graph state via tomography and classical correlations using post-selected data, since the systems do not support feed-forward operation. The fidelity of the four-qubit state consisting of two crossing-over cluster state is 0.41 ± 0.01 on the real devices with post-selection. The fidelity of each pair is 0.57 ± 0.01 and 0.58 ± 0.01 . Attempted verification of entanglement using Clauser-Horne-Shimony-Holt (CHSH) inequality experiments yields S values of 1.165 ± 0.04 and 1.235 ± 0.04 for two equivalent Bell pairs. Although not yet good enough for use in an algorithm, these results point the way to using quantum network coding both across networks and within systems.

I. INTRODUCTION

Quantum communication [1–4] is a promising field of study which has various applications, such as quantum cryptography [5–7] and distributed quantum computing [8]. However, the transmission of quantum information over long distances is a significant challenge due to loss in optical channels and the sensitivity of quantum states to the environment. In order to preserve fidelity many methods have been proposed, e.g., quantum error correction [9] and purification [10]. Combining methods for managing loss at the link layer [11–15] with these error management techniques and entanglement swapping leads to quantum repeaters [16–19].

Of course, a practical quantum network requires a complex network topology interconnecting many sites. Efficiently transmitting information across a complex network requires routing (selecting a path through the network) [20–24] and management of the available resources when multiple users are concurrently requesting use of the network [25]. Classical and quantum networks exhibit similar problems; for example, congestion arising at a bottleneck of the network [26]. One solution to contention for access to a channel is network coding [27]. The basic model is a butterfly network (Fig. 1). Similarly, in quantum communication, quantum network coding can be used to overcome the topological limits of the network. Inspired by quantum network coding (QNC) and measurement-based quantum computing, in 2018 Matsuo *et al.* introduced measurement-based quantum network coding (MQNC) [28]. Instead of relying on a Bell-pair based approach, measurement-based quantum network

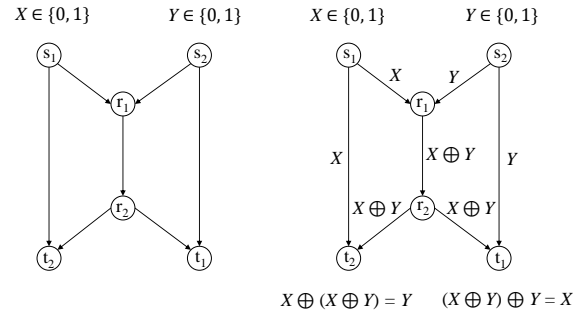


FIG. 1: The left figure shows the butterfly network topology where s_1 and s_2 each want to send a bit to t_1 and t_2 respectively. Right figure shows the classical network coding procedure using XOR operation to encode and decode the messages.

coding builds a graph or cluster state and performs network coding on top of this single entangled state. In this paper, we present our implementation, measurement and analysis of MQNC on an IBMQ device.

To formally address the problem, imagine (classical) senders s_1 and s_2 simultaneously want to send messages X and Y respectively, assuming that X and Y are both one bit of data, to their corresponding target receiver, t_1 , t_2 , across a bottleneck r_1 and r_2 . One trivial solution is for senders to alternate use of the channel. One sender waits until the other sender successfully sends his message, takes its turn, then relinquishes the channel. Known as time division multiplexing (TDM), this simple method may under-utilize resources in a complex real-world network, forcing memories to wait and some channels to idle. Network coding, in contrast, can complete the transmission of two messages in one cycle, by encoding two incoming messages using an XOR operation at node r_1 , then sending the encoded message to both target nodes. The remaining task is to decode the message using another XOR operation and the one message received directly from another sender [27].

^{*} Department of Physics, Faculty of Science, Mahidol University, Bangkok 10400, Thailand.

[†] Keio University Shonan Fujisawa Campus, 5322 Endo, Fujisawa, Kanagawa 252-0882, Japan.

[‡] Keio University Shonan Fujisawa Campus, 5322 Endo, Fujisawa, Kanagawa 252-0882, Japan.
 corresponding author's email: rdv@sfc.wide.ad.jp

Analogous to their classical counterparts, various quantum network coding protocols have been proposed [23, 29]. Quantum network coding is primarily aimed at resource efficiency. Classical network coding has a broad range of applicability, but QNC shows an advantage over TDM in a narrower set of cases. However, it also allows us to defer routing decisions and combine communication with computation [30, 31].

This concept has been addressed analytically [30, 32–36]. Early work examined only pure states. Satoh *et al.* and Matsuo *et al.* showed the importance of decoherence via analysis and simulation [28, 36]. Here, we take a step toward real-world use via a proof-of-concept implementation on a real superconducting quantum computer, IBMQ Experience device. We assess the practical implications for the use of network coding within single systems as a data movement optimization, and in wide-area networks.

We implemented MQNC by using post-selection on a 6-qubit cluster state instead of classical feed-forward, due to hardware limitations on the IBMQ machines. As an alternative to traditional entanglement swapping, we also investigate distribution of entanglement using measurement-based quantum computing.

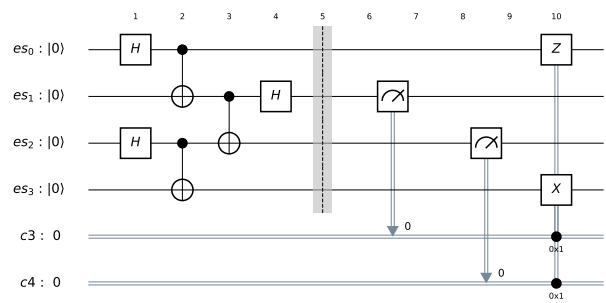
This paper is organized as follows. In section II, we briefly introduce measurement-based quantum computing, quantum network coding, measurement-based quantum network coding and linear cluster states for long-distance communication. We present experimental results for linear cluster states in section III then implement and analyze of the 6-qubit cluster state part of MQNC in section IV. Finally, we conclude the discussion in section V.

II. BACKGROUND

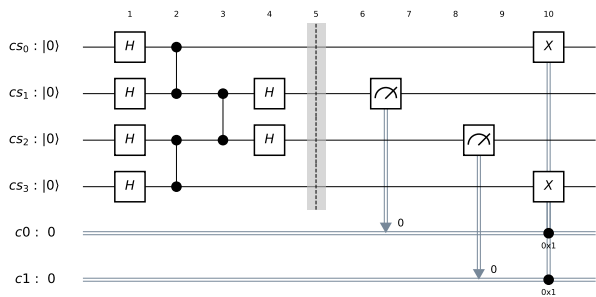
Quantum computation, whether conducted within a monolithic quantum computer, within a quantum multi-computer [37] or across a network, requires us to execute gates between qubits initially held some distance apart. Within a single computer, this can be done by moving qubits by shuttling ions or using SWAP gates to bring the qubits into proximity [38]. Once the qubits are brought together, two-qubit gates can be executed directly.

Alternatively, we can build distributed quantum states (e.g., Bell states) that span the distance, and use those distributed states either to teleport data [39] or to execute gates remotely [40, 41]. If the qubits are more than one site apart, we can build entanglement spanning that distance via entanglement swapping [42]. This can also be achieved via linear graph states and measurement-based computation [31].

When the system size exceeds the capacity of a single computer, we can couple together multiple computers over optical links. While the ideal is to transfer the state of a qubit to a photon and send it from one computer to the other, optical conversion and channel losses make



(a) Entanglement Swapping



(b) 4-qubit cluster state. X -measurement on two center qubits will result in 2-qubit cluster state.

FIG. 2: (a) Entanglement Swapping quantum circuit. (b) 2-qubit cluster state quantum circuit via X -measurement using 4-qubit cluster state.

that impossible. Thus, we use entanglement swapping and either purification or quantum error correction and build *quantum repeaters* [16].

All of these methods can be used as appropriate, when the needed resources are otherwise idle. However, when multiple operations need to happen across a topologically complex structure, *contention* for resources can lead to *congestion*, and force us to either alternate uses (multiplexing) [25] or build graph states that support quantum network coding.

In this section, we provide a brief introduction to each of these methods, before examining linear, contention-free communication on the IBMQ processors in Sec. III and the two methods for handling contention in Sec. IV.

A. Quantum state swapping using SWAP gate

With the constraint of device topology, swapping of the quantum state of two connected qubits is needed in order to proceed for further computation for 2-qubit operation using SWAP gates.

B. Entanglement swapping

Within a quantum computer, to entangle two qubits, first, apply a Hadamard operation on either one of them

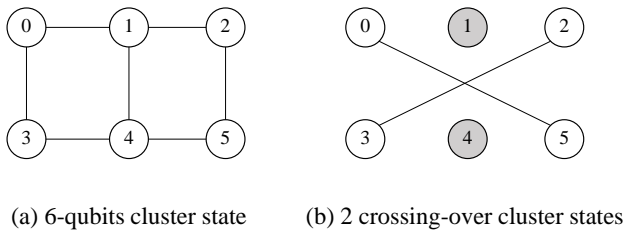


FIG. 3: By performing an X -measurement on qubits 1 and 4 on the cluster state in the left figure, two independent cluster states will be created as in the right figure.

then perform a Controlled- X operation using the other qubit as the target qubit. Now assume that there are two pairs of entangled qubits (Fig. 2) for es_0 entangled with es_1 and es_2 entangled with es_3 . Entanglement swapping can then be performed by applying a Controlled- X operation on es_1 (control qubit) and es_2 (target qubit) then applying a Hadamard operation on es_1 and measuring es_1 and es_2 in the computational basis. The measurement result must be sent through the classical channel to the receiver so that they can apply a byproduct operation to fix the quantum state. Therefore, information cannot travel faster than the speed of light.

C. Linear Cluster State for Long-Distance Communication

A linear graph state is an alternative to entanglement swapping. By performing Pauli measurements and byproduct operations on the qubits, which act as nodes in the network, we can transform the topology of a graph state. Notice that two and three-qubit graph states are LOCC equivalent to a Bell pair and GHZ state. Therefore, the linear graph state can be used to achieve the same objective as entanglement swapping.

D. Measurement-based Quantum Computing

Measurement-based quantum computing (MBQC), proposed by Raussendorf et al. in 2001 [31], is an alternative way of achieving universal quantum computation. MBQC uses sequential single-qubit measurements on the cluster state,

$$|G\rangle = \prod_{(a,b) \in E} CZ_{(a,b) \in E} |+\rangle^{\otimes n} \quad (1)$$

to perform the computation. E is a set of edges; a, b are corresponding vertices; and $CZ_{a,b}$ is a controlled- Z gate acting on qubits a and b .

After each measurement, a byproduct operation may be needed in order to fix the state into the desired state.

The byproduct operation will be determined by the measurement result of the qubit being measured. For example, by performing X -measurements on the bottleneck qubits and applying X operations dependent on the measurement results to the neighboring qubits, the original 6-qubit cluster state will be reduced to two 2-qubit cluster states, as in Fig. 3b.

E. Measurement-based Quantum Network coding

Based on MBQC and quantum network coding for quantum repeaters [36], in a simple case like a butterfly network, MQNC aims to create two crossing-over cluster states (Fig. 4d) by assuming an initial shared resource (Fig. 4a). A first step is merely entangling qubits. The second step removes qubits via Y -measurement, consequently creating a link between neighboring qubits, resulting in a 6-qubit cluster state. The final step is to remove qubits at the bottleneck of the network via X measurement resulting in 2 crossing-over cluster states. Either X measurement or Y measurement is required as the byproduct operation to correct the quantum state.

III. LINEAR COMMUNICATION ON THE IBMQ

The experiments in this paper were performed using the pure state QASM simulator, providing an ideal result, and real IBMQ Experience devices. Each trial consisted of 8192 shots. The circuit was optimized and the variable qubits mapped to the physical qubits by the QISKit transpiler. The IBMQ Experience devices are superconducting quantum computers that are available for use across the Internet via a web-based interface or programs in Python using QISKit libraries [43]. The devices used in this paper are IBMQ 20 Tokyo and IBMQ Poughkeepsie, each having 20 qubits as shown in Fig. 5.

We evaluate the performance of the real IBMQ devices by computing the fidelity $F = \langle \psi | \rho | \psi \rangle$ of the final reconstructed mixed state ρ obtained from QISKit state tomography with respect to the ideal pure state $|\psi\rangle$.

Performing the 6-qubit cluster state model on real devices require us to be concerned about fidelity loss along the process. To determine the expected fidelity as we add each qubit to the cluster state, we used a linear cluster state on the connected qubits of real devices. Since the devices do not support feed-forward operation, after executing a quantum circuit, data filtering is needed in order to obtain a feed-forward equivalent result, i.e., post-selection. We are assuming that there is no contention for resources. For example, consider the quantum circuit in Fig. 7, data with the measurement result of qubit 1 and 4 is '1' is being selected for further analysis.

Either moving qubits via SWAP gates or executing a remote gate via a nested sequence that utilizes intermediate qubits is necessary on the IBM today. There are

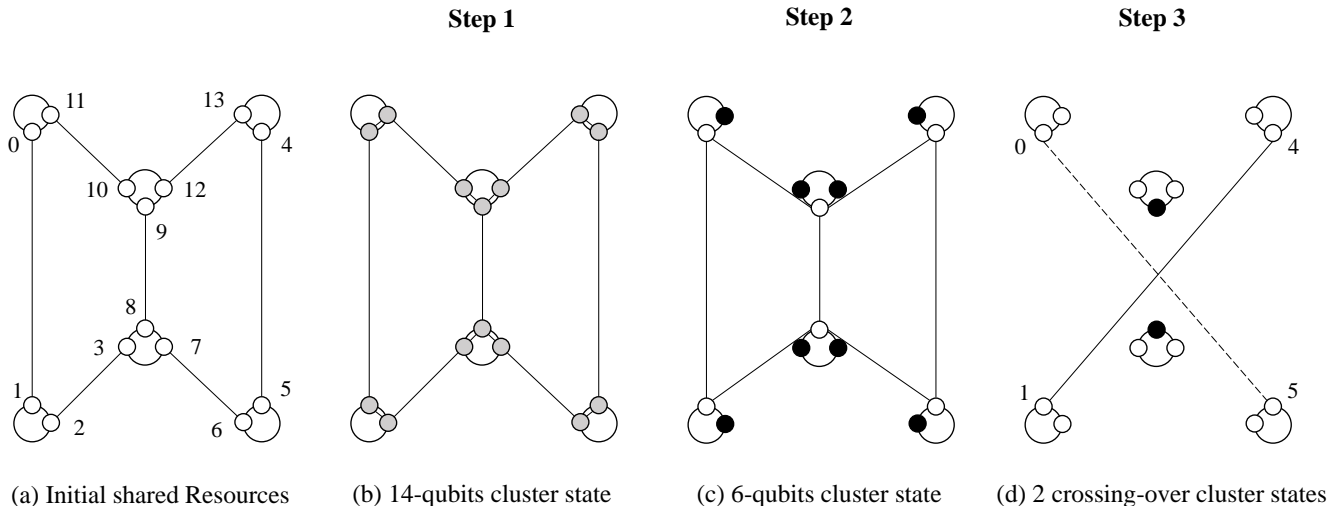


FIG. 4: MQNC encoding procedure. On (a) assuming initial shared resources before beginning the procedure. Each large circle represents a network node. Each small circle represents a qubit, entangled across a channel as represented by a line. (b) Create a 14-qubit graph state by apply CZ operation within main nodes. (c) Remove black qubits node via Y -measurement resulting in 6-qubit cluster state. (d) Remove black qubits node via X -measurement resulting in 2 crossing-over cluster states

several options for compiling efficient circuits. Nishio et al.[38] examined the tradeoffs between various options, including error-aware compilation.

A. Entanglement Swapping

Consider a simple model of entanglement swapping. The objective is to create a Bell pair using two distant qubits; qubit 0 will entangle with qubit 11 at the end of the operation (see selected qubit 0, 5, 6 and 11 from Fig. 5a and corresponding quantum circuit in Fig. 2a). We also conducted an experiment using qubits 1, 5, 6 and 10. Qubits 1 and 10 will be entangled at the end of the operation. Using one trial with post-selection where the measurement results of qubits 5 and 6 are 0, we performed state-tomography to reconstruct the density matrix from the post-selected result. We find state fidelity ≈ 0.76 for qubit 0 and 11 and for qubit 1 and 10 ≈ 0.66 compared with the expected Bell pair

$$|\Phi^+\rangle = \frac{1}{\sqrt{2}}(|00\rangle + |11\rangle). \quad (2)$$

B. Linear cluster state

A cluster state can be easily prepared by initializing all qubits in the state $|+\rangle = \frac{1}{\sqrt{2}}(|0\rangle + |1\rangle)$ by applying the Hadamard operation on each qubit, then connecting each qubit via a controlled- Z operation in the desired topology.

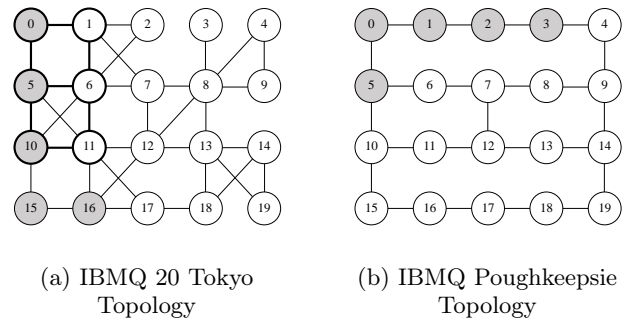


FIG. 5: IBMQ devices topology. Gray qubits indicate qubits chosen to perform state tomography of linear cluster state. IBMQ 20 Tokyo starts from qubit 0 to 16 and IBMQ Poughkeepsie starts from qubit 5 to qubit 3. Heavy lines indicate qubits used to create the 6-qubit cluster state on Tokyo for both state tomography and the correlation matrix.

To achieve the same objective as the entanglement swapping procedure in section III A, a 4-qubit linear cluster state can also be used to entangle distant qubits by performing X -measurements on the qubits at the center. This will directly link two remaining qubits together after apply byproduct operations (two set of qubits is the same as selected in III A and corresponding quantum circuit in Fig. 2b). Using one trial of post-selection for measurement results of 0 on qubit 5 and 6 and state-tomography, we find a state fidelity ≈ 0.70 for qubit 0 and 11, ≈ 0.63

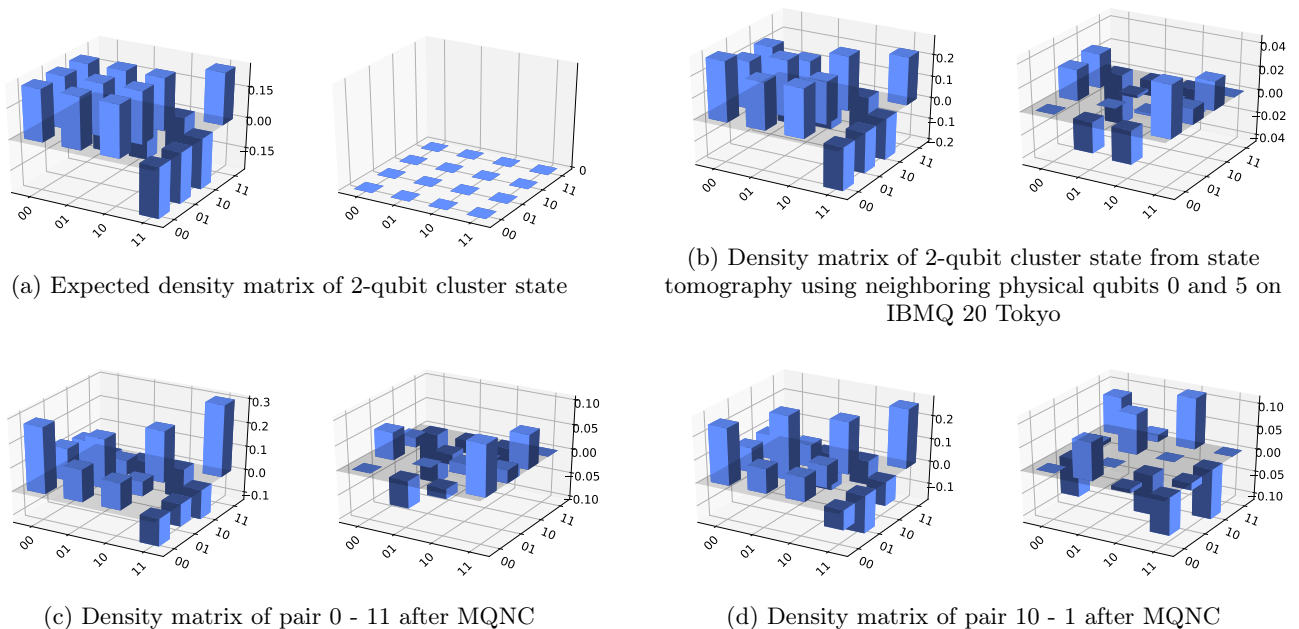


FIG. 6: In each figure, the real part of the density matrix is on the left and the imaginary part is on the right. (a) Expected density matrix of 2-qubit linear cluster state. (b) Reconstructed density matrix of directly created 2-qubit linear cluster state using physical qubits 0 and 5 on IBMQ 20 Tokyo. Note that the vertical scale of the imaginary component is small. (c) and (d) are reconstructed density matrices of pairs 0 - 11 and 10 - 1.

n qubits	IBMQ 20 Tokyo	IBMQ Poughkeepsie
2	0.876 ± 0.005	0.821 ± 0.013
3	0.695 ± 0.003	0.700 ± 0.023
4	0.405 ± 0.003	0.595 ± 0.017
5	0.150 ± 0.010	0.373 ± 0.018

TABLE I: Fidelity of n qubit linear cluster states on real devices

for qubit 1 and 10 compared with the ideal 2-qubit cluster state,

$$|\Psi\rangle = \frac{1}{\sqrt{2}}(|0+\rangle + |1-\rangle), \quad (3)$$

where $|-\rangle = \frac{1}{\sqrt{2}}(|0\rangle - |1\rangle)$. 2-qubit cluster state entanglement can turn into Bell pair in Eq. (2) via applying a Hadamard operation on either qubit.

From the topology of IBMQ 20 Tokyo, we selected qubits 0, 5, 10, 15 and 16. For IBMQ Poughkeepsie, we selected qubits 5, 0, 1, 2, and 3 (see Fig. 5 for devices topology). For state tomography, we performed five trials of 8192 shots each on n qubits after the construction of n qubits linear cluster state. The fidelity is as shown in Table I. For a sample result, a plot of the density matrix of the 2-qubit linear cluster state is shown in Fig. 6b. The results suggest that entanglement swapping achieves our objective with more fidelity than via MQNC scheme.

IV. QUANTUM NETWORK CODING ON THE IBMQ

In the previous section, we investigated the cases when there was no contention for resources. However, in real-world networks and in real physical systems, resource contention is inevitable and must be addressed. In this section we analyze an implementation of MQNC that is specifically designed to deal with resource contention in networks and in the systems such as IBMQ devices.

We implement the 6-qubit cluster state part of the MQNC protocol (Step 2 in Fig. 4) and evaluate the fidelity using state tomography on 2-crossing over cluster states to the ideal quantum state in a form of

$$|\Psi\rangle|\Psi\rangle = \left(\frac{1}{\sqrt{2}}(|0+\rangle + |1-\rangle)\right) \otimes \left(\frac{1}{\sqrt{2}}(|0+\rangle + |1-\rangle)\right). \quad (4)$$

Then, by using two 2-qubit cluster states which are turned into Bell pairs, we calculate a correlation matrix and violation of CHSH inequality.

A. Implementation on IBMQ 20 Tokyo

Following Step 2 of the MQNC procedure in Fig. 4 to create the 2 crossing over cluster states, the quantum circuit in Fig. 7 was executed on IBMQ 20 Tokyo. For the 6-qubit cluster state, qubits 0, 1, 5, 6, 10 and 11 were chosen in order to avoid the need for SWAP gates.

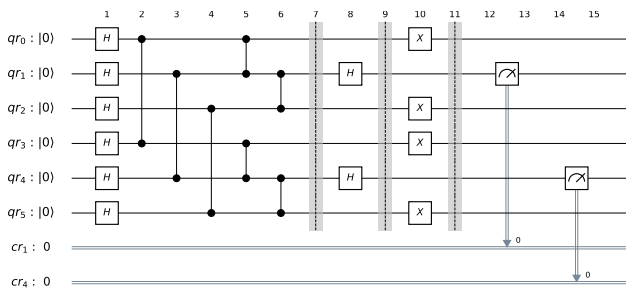


FIG. 7: 6-qubit cluster state quantum circuit for case of qubit 1 and qubit 4 resulting in '1', apply X operation on connected qubits

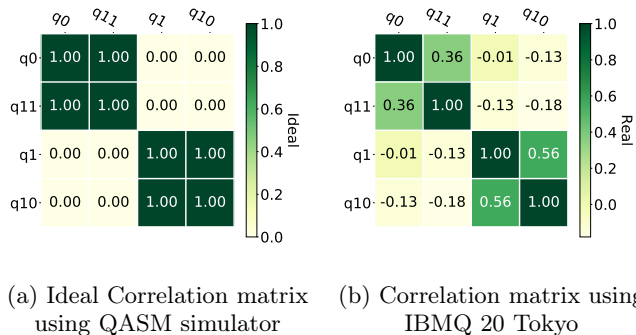


FIG. 8: (a) Correlation Matrix of 2 crossing-over entangle qubits using QASM simulator. (b) Correlation Matrix for classical measurement result of 2 crossing-over entangled qubits created from the 6-qubit cluster state on IBMQ 20 Tokyo. Standard deviation for the entangled and the non-entangled pairs was found to be approximately 0.02.

Qubits 0, 1 will be entangled with qubit 11, 10 respectively after the procedure. Virtual qubits 0, 1, 2, 3, 4 and 5 in Fig. 3 are mapped to physical qubits 0, 5, 10, 1, 6 and 11, respectively. The fidelity of the four-qubit state of 2 crossing over cluster states was found to be $\approx 0.41 \pm 0.01$ with respect to Eq. (4) with twenty trials of state tomography where measurement result of qubit 1 and 4 was post-selected to be '1'. The fidelity of the state on qubits 0 and 11 was found to be 0.57 ± 0.01 with respect to the ideal state in Eq. (3), and 0.58 ± 0.01 for the pair consisting of qubits 1 and 10.

B. Entanglement Verification

To further analyze the procedure, we calculate a correlation matrix for the four remaining qubits by turning each cluster state into a Bell pair. Fig. 8a, an ideal result using ten trials of the QASM simulator, shows that qubits 0, 11 and 1, 10 have correlation value 1, which shows the maximal correlation and other entries are almost 0. This implies that there is no correlation between

	pair	S Value
Entanglement pair	0 - 11	1.165 ± 0.04
	10 - 1	1.235 ± 0.04
Non-Entanglement pair	0 - 10	-0.405 ± 0.06
	0 - 1	-0.149 ± 0.03
	11 - 10	-0.326 ± 0.04
	11 - 1	-0.084 ± 0.06

TABLE II: S values of each qubit pair using IBMQ 20 Tokyo for 8 trials

those qubits as one would expect.

Fig. 8b is a correlation matrix using IBMQ 20 Tokyo with one hundred trials, showing a decline of correlation values from the ideal result. This should be expected from the fidelity of the state. However, the value for a pair expected to be entangled is significantly higher than a pair expected to be disentangled. The result from IBMQ 20 Tokyo reveals moderately large positive correlations where we expect them and significant negative correlations where we would hope for zero.

Entanglement verification can be done using the CHSH inequality [44]. In this simple case, to check whether two qubits are entangled with each other or not, in a series of trials, two different basis sets are used to measure each qubit: $A = X, A' = Z$ and $B = H, B' = ZHZ$. The cumulative measurement results are used to calculate the quantity,

$$S = \langle AB \rangle - \langle AB' \rangle + \langle A'B \rangle + \langle A'B' \rangle, \quad (5)$$

where $\langle AB \rangle = p_{00} + p_{11} - p_{01} - p_{10}$ is the correlation between observables A and B , and p_{01} is the probability of measuring '0' on the first qubit and '1' on the second qubit.

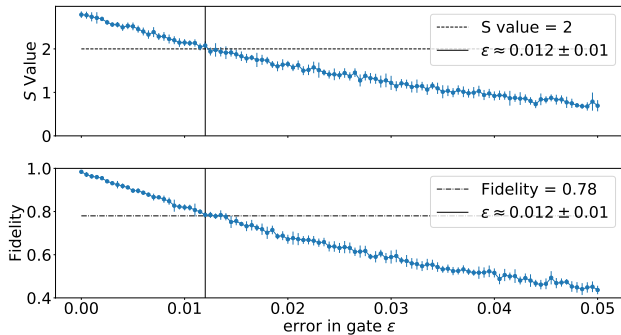
Table II shows the S values from each pair using eight trials of 8192 shots each and post-selecting where qubits 1 and 4 give measurement result to be '1'. The S value does not exceed 2 failing to conclusively demonstrate non-classical entanglement, but this is the result to be expected from a quantum state of this fidelity.

We model the final mixed state of the two entangled qubits as a Werner state [45],

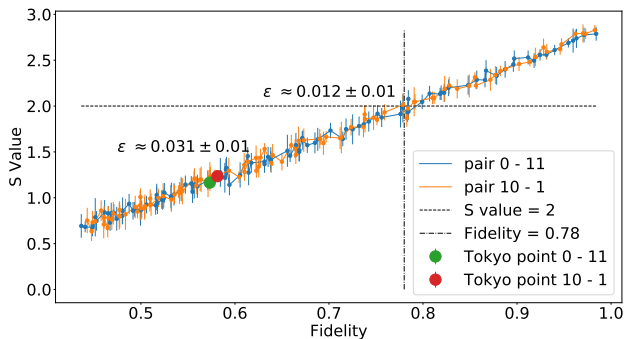
$$\rho_p^W = (1-p) |\Phi^+\rangle \langle \Phi^+| + p \frac{I}{4}, \quad (6)$$

where I is the identity operator and p is the total 2-qubit error rate at the end of the MQNC. From Ref. [46], we expect that the Werner state violates the CHSH inequality for $1-p > 1/\sqrt{2}$. The error rate p is related to the fidelity F via $F = (4-3p)/4$, so in order to violate the CHSH inequality we require final fidelity of at least $F \gtrsim 0.78$.

By using QISKit's noisy simulation, we vary the probability of an error ϵ using the depolarizing error from 0 to 0.05 (101 data points repeated 10 times each and 1024 shots per time) in one and two qubit gates which derive from error probability of one qubit gate. We simulate the 6-qubit butterfly part of MQNC twice, one for performing state tomography for 2 qubit and another for



(a) Using QISKit noisy simulator for pair 0 - 11, an upper figure is a plot between ϵ and S value, where vertical solid line indicate the approximate ϵ that give $S > 2$. A lower figure is a plot between ϵ and fidelity which dot-dash line indicate a value corresponding to ϵ that give $S > 2$.



(b) Combining plot of fidelity and corresponding S value with the same ϵ . Green and red points are the data from IBMQ 20 Tokyo.

FIG. 9: Fidelity and corresponding S value using QISKit noisy simulation.

CHSH experiment by turning two crossing-over cluster states into Bell pairs. The result from the simulation is sorted by fidelity and plotted against the S value from CHSH experiment in Fig. 9b. It shows that the noise model in Eq. (6) is adequate because both data points from IBMQ 20 Tokyo are on the predicted curve using the noisy QASM simulator. The two data points do not have sufficiently high fidelity to violate the CHSH inequality. We can extrapolate the critical single-qubit error rate ϵ_{crit} which results in a CHSH violation. Fig. 9b suggest that $\epsilon_{crit} \approx 1.2\%$ which is less than half of the depolarising error rate of the 2 data points obtained from IBMQ 20 Tokyo.

V. DISCUSSION

In this paper, we have taken a step from the theory of quantum network coding toward practical use on real devices. By implementing and comparing to more tradi-

tional entanglement swapping and to linear cluster states, we can assess the conditions under which each of the three approaches will best serve applications. This will benefit multiple applications competing for access to a network, as well as help us to coordinate use of resources inside a single quantum system as part of the algorithm compilation and optimization process. Of course, a common usage scenario in networks is to assume each link is a long-distance optical channel and we are implementing QNC in a distributed fashion. An alternative use inside a single system might be switching longer-distance connections when the system is used as a quantum router in a network.

Experimentally, we have found that QNC is not yet achievable on the machine named Tokyo. After the completion of the QNC, we should be left with two independent two-qubit cluster states, but the six-qubit entanglement may or may not give us complete independence due to imperfections in the state creation and measurement. To check, in addition to calculating the CHSH inequality for the qubit pairs we *expect* to be entangled, we also calculated S for qubit pairs we expect to *not* be entangled—each term in Eq. (5) should be ≈ 0 if the two qubits are completely independent. The values in Fig. 8b and II suggest that residual entanglement remains after post-selection. Of course, post-selection only emulates the full behavior of QNC; actual measurement and feed-forward would produce different results, but our data here is suggestive. Poughkeepsie, a newer machine, is higher fidelity but its interconnection topology is not rich enough to directly implement QNC. The rapid improvements in hardware suggest that QNC will violate the CHSH inequality within a generation or two, if the processor topology allows.

A next step is to simulate incorporating photon loss of stochastic behavior with and without competing traffic on a large network. Further evaluation of the utility of both linear graph-based teleportation and QNC on monolithic quantum computer await the arrival of feed-forward functionality. This points the way to hybrid measurement/gate-based quantum computation.

ACKNOWLEDGEMENT

This material is based upon work supported by the Air Force Office of Scientific Research under award number FA2386-19-1-4038. The results presented in this paper were obtained in part using an IBM Q quantum computing system as part of the IBM Q Network. The views expressed are those of the authors and do not reflect the official policy or position of IBM or the IBM Q team.

Appendix A: QISKit Version

The version of QISKit packages we use are listed in Table III.

name	version
qiskit	0.10.5
qiskit-terra	0.8.2
qiskit-ignis	0.1.1
qiskit-aer	0.2.1
qiskit-ibmq-provider	0.2.2
qiskit-aqua	0.5.2

TABLE III: QISKit packages version

Appendix B: Date-time

Each experiment was performed on the dates listed in Table IV.

Experiment	Date-time
4 qubit Entanglement Swapping and 4 qubit Linear Cluster state on IBMQ 20 Tokyo	2019/7/24
n -qubit Linear Cluster on IBMQ 20 Tokyo	2019/8/21-22
n -qubit Linear Cluster on IBMQ Poughkeepsie	2019/8/27-28
6 qubit cluster state fidelity on IBMQ 20 Tokyo	2019/8/25-27
Correlation Matrix of 2 crossing-over pairs on IBMQ 20 Tokyo	2019/8/27
CHSH inequality of 2 crossing-over pairs on IBMQ 20 Tokyo	2019/8/24

TABLE IV: Date and time when experimental data have been taken

-
- [1] S. Wehner, D. Elkouss, and R. Hanson, *Science* **362** (2018), 10.1126/science.aam9288, .
- [2] H. J. Kimble, *Nature* **453**, 1023 (2008).
- [3] S. Muralidharan, L. Li, J. Kim, N. Lütkenhaus, M. D. Lukin, and L. Jiang, *Scientific Reports* **6**, 20463 (2016).
- [4] R. Van Meter, *Quantum Networking* (Wiley-ISTE, 2014).
- [5] C. H. Bennett and G. Brassard, in *Proc. IEEE International Conference on Computers, Systems, and Signal Processing* (IEEE, 1984) pp. 175–179.
- [6] A. Ekert, *Physical Review Letters* **67**, 661 (1991).
- [7] C. Elliott, D. Pearson, and G. Troxel, in *Proc. SIGCOMM 2003*, ACM (ACM, 2003).
- [8] H. Buhrman and H. Röhrig, “Mathematical foundations of computer science 2003,” (Springer-Verlag, 2003) Chap. Distributed Quantum Computing, pp. 1–20.
- [9] S. J. Devitt, W. J. Munro, and K. Nemoto, *Reports on Progress in Physics* **76**, 076001 (2013).
- [10] W. Dür, H. Aschauer, and H.-J. Briegel, *Phys. Rev. Lett.* **91**, 107903 (2003).
- [11] A. Dahlberg, M. Skrzypczyk, T. Coopmans, L. Wubben, F. Rozpędek, M. Pompili, A. Stolk, P. Pawełczak, R. Knegjens, R. Hanson, *et al.*, arXiv preprint arXiv:1903.09778 (2019).
- [12] T. Matsuo, C. Durand, and R. Van Meter, arXiv preprint arXiv:1904.08605 (2019).
- [13] C. Jones, D. Kim, M. T. Rakher, P. G. Kwiat, and T. D. Ladd, *New Journal of Physics* **18**, 083015 (2016).
- [14] P. C. Humphreys, N. Kalb, J. P. Morits, R. N. Schouten, R. F. Vermeulen, D. J. Twitchen, M. Markham, and R. Hanson, *Nature* **558**, 268 (2018).
- [15] V. Krutyanskiy, M. Meraner, J. Schupp, V. Krcmarsky, H. Hainzer, and B. Lanyon, *npj Quantum Information* **5**, 72 (2019).
- [16] W. Dür, H.-J. Briegel, J. I. Cirac, and P. Zoller, *Phys. Rev. A* **59**, 169 (1999).
- [17] M. Zwerger, A. Pirker, V. Dunjko, H. J. Briegel, and W. Dür, *Phys. Rev. Lett.* **120**, 030503 (2018).
- [18] L. Jiang, J. M. Taylor, K. Nemoto, W. J. Munro, R. Van Meter, and M. D. Lukin, *Phys. Rev. A* **79**, 032325 (2009).
- [19] A. G. Fowler, D. S. Wang, C. D. Hill, T. D. Ladd, R. Van Meter, and L. C. L. Hollenberg, *Phys. Rev. Lett.* **104**, 180503 (2010).
- [20] R. Van Meter, T. Satoh, T. D. Ladd, W. J. Munro, and K. Nemoto, *Networking Science* **3**, 82 (2013).
- [21] M. Caleffi, *IEEE Access* **5**, 22299 (2017).
- [22] E. Schoute, *Shortcuts to quantum network routing*, Master’s thesis, T.U. Delft (2015).
- [23] M. Pant, H. Krovi, D. Towsley, L. Tassiulas, L. Jiang, P. Basu, D. Englund, and S. Guha, *npj Quantum Information* **5**, 25 (2019).
- [24] L. Gyongyosi and S. Imre, *Scientific reports* **7**, 14255 (2017).
- [25] L. Aparicio and R. Van Meter, in *Proc. SPIE*, Vol. 8163 (2011) p. 816308.
- [26] V. Jacobson, in *Symposium proceedings on Communications architectures and protocols*, SIGCOMM ’88 (ACM, New York, NY, USA, 1988) pp. 314–329.
- [27] R. Ahlswede, N. Cai, S. Li, and R. Yeung, *Information Theory*, *IEEE Transactions on* **46**, 1204 (2000).
- [28] T. Matsuo, T. Satoh, S. Nagayama, and R. Van Meter, *Phys. Rev. A* **97**, 062328 (2018).
- [29] B. K. Behera, T. Reza, A. Gupta, and P. K. Panigrahi, *Quantum Information Processing* **18**, 328 (2019).
- [30] S. Akibue and M. Murao, *IEEE Transactions on Information Theory* **62**, 6620 (2016).
- [31] R. Raussendorf and H. J. Briegel, *Phys. Rev. Lett.* **86**, 5188 (2001).
- [32] M. Hayashi, K. Iwama, H. Nishimura, R. Raymond, and S. Yamashita, in *STACS 2007*, edited by W. Thomas and P. Weil (Springer Berlin Heidelberg, Berlin, Heidelberg, 2007) pp. 610–621.
- [33] K. Iwama, H. Nishimura, R. Raymond, and S. Yamashita, Arxiv preprint quant-ph/0611039 (2006).
- [34] D. Leung, J. Oppenheim, and A. Winter, *IEEE Trans. Inf. Theor.* **56**, 3478 (2010).
- [35] T. Satoh, K. Ishizaki, S. Nagayama, and R. Van Meter, *Phys. Rev. A* **93**, 032302 (2016).
- [36] T. Satoh, F. m. c. Le Gall, and H. Imai, *Phys. Rev. A* **86**, 032331 (2012).

- [37] R. Van Meter, W. J. Munro, K. Nemoto, and K. M. Itoh, *J. Emerg. Technol. Comput. Syst.* **3**, 2:1 (2008).
- [38] S. Nishio, Y. Pan, T. Satoh, H. Amano, and R. Van Meter, “Extracting Success from IBM’s 20-Qubit Machines Using Error-Aware Compilation,” (2019), arXiv:1903.10963v1.
- [39] C. H. Bennett, G. Brassard, C. Crépeau, R. Jozsa, A. Peres, and W. K. Wootters, *Phys. Rev. Lett.* **70**, 1895 (1993).
- [40] J. Eisert, K. Jacobs, P. Papadopoulos, and M. Plenio, *Physical Review A* **62**, 52317 (2000).
- [41] D. Gottesman and I. L. Chuang, *Nature* **402**, 390 (1999).
- [42] J.-W. Pan, D. Bouwmeester, H. Weinfurter, and A. Zeilinger, *Phys. Rev. Lett.* **80**, 3891 (1998).
- [43] H. Abraham, I. Y. Akhalwaya, G. Aleksandrowicz, T. Alexander, G. Alexandrowics, E. Arbel, A. Asfaw, C. Azaustre, P. Barkoutsos, G. Barron, L. Bello, Y. Ben-Haim, L. S. Bishop, S. Bosch, D. Bucher, CZ, F. Cabrera, P. Calpin, L. Capelluto, J. Carballo, C.-F. Chen, A. Chen, R. Chen, J. M. Chow, C. Claus, A. W. Cross, A. J. Cross, J. Cruz-Benito, Cryoris, C. Culver, A. D. Córcoles-Gonzales, S. Dague, M. Dartiailh, A. R. Davila, D. Ding, E. Dumitrescu, K. Dumon, I. Duran, P. Eendebak, D. Egger, M. Everitt, P. M. Fernández, A. Frisch, A. Fuhrer, J. Gacon, Gadi, B. G. Gago, J. M. Gambetta, L. Garcia, S. Garion, Gawel-Kus, L. Gil, J. Gomez-Mosquera, S. de la Puente González, D. Greenberg, J. A. Gunnels, I. Haide, I. Hamamura, V. Havlicek, J. Hellmers, L. Herok, H. Horii, C. Howington, W. Hu, S. Hu, H. Imai, T. Imamichi, R. Iten, T. Itoko, A. Javadi-Abhari, Jessica, K. Johns, N. Kanazawa, A. Karazeev, P. Kassebaum, V. Krishnan, K. Krsulich, G. Kus, R. LaRose, R. Lambert, J. Latone, S. Lawrence, P. Liu, P. B. Z. Mac, Y. Maeng, A. Malyshev, J. Marecek, M. Marques, D. Mathews, A. Matsuo, D. T. McClure, C. McGarry, D. McKay, S. Meesala, A. Mezzacapo, R. Midha, Z. Minev, R. Morales, P. Murali, J. Müggenburg, D. Nadlinger, G. Nannicini, P. Nation, Y. Naveh, Nick-Singstock, P. Niroula, H. Norlen, L. J. O’Riordan, P. Ollitrault, S. Oud, D. Padilha, H. Paik, S. Perriello, A. Phan, M. Pistoia, A. Pozas-iKerstjens, V. Prutyaynov, J. Pérez, Quintiii, R. Raymond, R. M.-C. Redondo, M. Reuter, D. M. Rodríguez, M. Ryu, M. Sandberg, N. Sathaye, B. Schmitt, C. Schnabel, T. L. Scholten, E. Schoute, I. F. Sertage, Y. Shi, A. Silva, Y. Siraichi, S. Sivrajah, J. A. Smolin, M. Soeken, D. Steenken, M. Stypulkoski, H. Takahashi, C. Taylor, P. Taylour, S. Thomas, M. Tillet, M. Tod, E. de la Torre, K. Trabing, M. Treinish, TrishaPe, W. Turner, Y. Vaknin, C. R. Valcarce, F. Varchon, D. Vogt-Lee, C. Vuillot, J. Weaver, R. Wieczorek, J. A. Wildstrom, R. Wille, E. Winston, J. J. Woehr, S. Woerner, R. Woo, C. J. Wood, R. Wood, S. Wood, J. Wootton, D. Yeralin, J. Yu, L. Zdanski, Zoufalc, anedumla, azulehner, bcamorrison, drholmie, fanizzamarco, kanejess, klinvill, merav aharoni, ordmoj, tigerjack, yang.luh, and yotamvakninibm, “Qiskit: An open-source framework for quantum computing,” (2019).
- [44] J. F. Clauser, M. A. Horne, A. Shimony, and R. A. Holt, *Phys. Rev. Lett.* **23**, 880 (1969).
- [45] R. F. Werner, *Phys. Rev. A* **40**, 4277 (1989).
- [46] T. Vértesi, *Phys. Rev. A* **78**, 032112 (2008).